AFRL-VA-WP-TP-2006-330

FLIGHT CONTROL OF HYPERSONIC SCRAMJET VEHICLES USING A DIFFERENTIAL ALGEBRAIC APPROACH (POSTPRINT)

Tony A. Adami, J. Jim Zhu, Michael A. Bolender, David B. Doman, and Michael W. Oppenheimer

AUGUST 2006

Approved for public release; distribution is unlimited.

STINFO COPY

AIR VEHICLES DIRECTORATE
AIR FORCE MATERIEL COMMAND
AIR FORCE RESEARCH LABORATORY
WRIGHT-PATTERSON AIR FORCE BASE, OH 45433-7542

NOTICE AND SIGNATURE PAGE

Using Government drawings, specifications, or other data included in this document for any purpose other than Government procurement does not in any way obligate the U.S. Government. The fact that the Government formulated or supplied the drawings, specifications, or other data does not license the holder or any other person or corporation; or convey any rights or permission to manufacture, use, or sell any patented invention that may relate to them.

This report was cleared for public release by the Air Force Research Laboratory Wright Site (AFRL/WS) Public Affairs Office and is available to the general public, including foreign nationals. Copies may be obtained from the Defense Technical Information Center (DTIC) (http://www.dtic.mil).

AFRL-VA-WP-TP-2006-330 HAS BEEN REVIEWED AND IS APPROVED FOR PUBLICATION IN ACCORDANCE WITH ASSIGNED DISTRIBUTION STATEMENT.

*//Signature//

David B. Doman
Senior Aerospace Engineer
Control Design and Analysis Branch
Air Force Research Laboratory
Air Vehicles Directorate

//Signature//

James H. Myatt
Acting Chief
Control Design and Analysis Branch
Air Force Research Laboratory
Air Vehicles Directorate

//Signature//

JEFFREY C. TROMP
Senior Technical Advisor
Control Sciences Division
Air Vehicles Directorate

This report is published in the interest of scientific and technical information exchange, and its publication does not constitute the Government's approval or disapproval of its ideas or findings.

*Disseminated copies will show "//Signature//" stamped or typed above the signature blocks.

REPORT DOCUMENTATION PAGE

Form Approved
OMB No. 0704-0188

1. REPORT DATE *(DD-MM-YY)*	2. REPORT TYPE	3. DATES COVERED *(From - To)*
August 2006	Conference Paper Postprint	06/15/2005 – 07/31/2006

4. TITLE AND SUBTITLE
FLIGHT CONTROL OF HYPERSONIC SCRAMJET VEHICLES USING A DIFFERENTIAL ALGEBRAIC APPROACH (POSTPRINT)

5a. CONTRACT NUMBER In-house

5b. GRANT NUMBER

5c. PROGRAM ELEMENT NUMBER 62201F

6. AUTHOR(S)
Tony A. Adami and J. Jim Zhu (Ohio University)
Michael A. Bolender, David B. Doman, and Michael W. Oppenheimer (AFRL/VACA)

5d. PROJECT NUMBER N/A

5e. TASK NUMBER N/A

5f. WORK UNIT NUMBER N/A

7. PERFORMING ORGANIZATION NAME(S) AND ADDRESS(ES)

Ohio University
Athens, OH 45701

Control Design and Analysis Branch (AFRL/VACA)
Control Sciences Division
Air Vehicles Directorate
Air Force Materiel Command, Air Force Research Laboratory
Wright-Patterson Air Force Base, OH 45433-7542

8. PERFORMING ORGANIZATION REPORT NUMBER
AFRL-VA-WP-TP-2006-330

9. SPONSORING/MONITORING AGENCY NAME(S) AND ADDRESS(ES)

Air Vehicles Directorate
Air Force Research Laboratory
Air Force Materiel Command
Wright-Patterson Air Force Base, OH 45433-7542

10. SPONSORING/MONITORING AGENCY ACRONYM(S)
AFRL-VA-WP

11. SPONSORING/MONITORING AGENCY REPORT NUMBER(S)
AFRL-VA-WP-TP-2006-330

12. DISTRIBUTION/AVAILABILITY STATEMENT
Approved for public release; distribution is unlimited.

13. SUPPLEMENTARY NOTES
The U.S. Government is joint author of the work and has the right to use, modify, reproduce, release, perform, display, or disclose the work.

Conference paper published in the Proceedings of the AIAA Guidance, Navigation, and Control Conference and Exhibit, published by AIAA. PAO Case Number: AFRL/WS 06-1950 (cleared August 19, 2006).

14. ABSTRACT
Trajectory Linearization Control is applied to the longitudinal hypersonic scramjet vehicle model under development at the Air Force Research Laboratory. The algorithm is based on Differential Algebraic Spectral Theory which features a time-varying eigenvalue concept and avoids the use of so-called frozen-time eigenvalues which can lead to unreliable results when applied to time-varying dynamics systems. A trajectory linearization control was first designed for a non-linear, affine, rigid-body model using an allocation strategy based on trim-condition look-up tables formulated by trimming the model at multiple operating points while varying velocity and altitude. This data was then fitted to a polynomial function, and the lookup tables were replaced by analytical expressions for the effector settings. The TLC design was then verified on the first-principles based, longitudinal, rigid-body hypersonic vehicle model developed at AFRL using both look-up table and curve fit strategies, and simulation testing results are presented. The current design will be further extended to allow adaptive control of time-varying flexible modes using time-varying bandwidth notch filters and a trajectory linearization observer.

15. SUBJECT TERMS

16. SECURITY CLASSIFICATION OF: a. REPORT	b. ABSTRACT	c. THIS PAGE	17. LIMITATION OF ABSTRACT:	18. NUMBER OF PAGES	19a. NAME OF RESPONSIBLE PERSON (Monitor)
Unclassified	Unclassified	Unclassified	SAR	26	David B. Doman
					19b. TELEPHONE NUMBER *(Include Area Code)* N/A

Standard Form 298 (Rev. 8-98)
Prescribed by ANSI Std. Z39-18

Flight Control of Hypersonic Scramjet Vehicles Using a Differential Algebraic Approach

Tony A. Adami* and J. Jim Zhu †
Ohio University, Athens, Ohio, 45701

Michael A. Bolender‡ , David B. Doman§ , and Michael Oppenheimer¶
Air Force Research Laboratory, Wright Patterson AFB, OH 45433

[Abstract] Trajectory Linearization Control (TLC) is applied to a longitudinal hypersonic scramjet vehicle (HSV) model. The TLC algorithm is based on Differential Algebraic Spectral Theory (DAST) which features a time-varying eigenvalue concept and avoids the use of so-called frozen-time eigenvalues that can lead to unreliable results when applied to time-varying dynamical systems. A TLC controller was first designed for a nonlinear, affine, rigid-body model using an allocation strategy based on trim-condition lookup tables. The tables were populated by trimming the model at multiple operating points while varying velocity and altitude. The trim data was then fitted to a cubic polynomial function, and the lookup tables were replaced by analytical expressions for the effector settings. The TLC design was then verified on a first-principles based, longitudinal, rigid-body hypersonic vehicle model, and initial simulation testing results are presented.

Nomenclature

x	= State vector
μ	= Control vector
η	= Output vector
h	= Altitude
γ	= Flight path angle
V_t	= Velocity
θ	= Pitch angle
Q	= Body pitch rate
α	= Angle of attack
L	= Total lift
T	= Total thrust
M_y	= Pitch Moment
L_{aero}	= Aerodynamic lift
D_{aero}	= Aerodynamic drag
F_{prop}	= Propulsion force
L_{prop}	= Lift due to propulsion
D_{prop}	= Drag due to propulsion
L_{ctrl}	= Lift due to elevator deflection
D_{ctrl}	= Drag due to elevator deflection
M_o	= Mach number
δ_{th}	= fuel equivalence ratio
δ_e	= elevator deflection

---

* PhD Candidate, Electrical Engineering and Computer Science, Ohio University, Student Member AIAA
† Professor, Electrical Engineering and Computer Science, Ohio University, Professional Member AIAA
‡ Aerospace Engineer, Senior Member AIAA
§ Senior Aerospace Engineer, Associate Fellow AIAA.
¶ Electronics Engineer, Member AIAA

I. Introduction

Hypersonic Scramjet Vehicle (HSV) technology has become attractive in recent years as a possible launch vehicle solution. Current launch costs (approximately $10,000/lb) are prohibitive, and Scramjet vehicles offer significant relief by utilizing oxygen in the atmosphere for combustion, thus greatly reducing launch weight. A combined-cycle approach is eventually envisioned using a vehicle that can alter its propulsion method based on flight conditions. High-speed travel and delivery of cargo (i.e. global overnight delivery) is another potential application for HSV's.

Research and development in this area is currently focusing on several key challenges arising from the unique integration of airframe, propulsion system, and flight control system of HSV's. The supersonic velocities attained by the air flowing through the combustor dictate a long, slender vehicle fuselage, thus inevitably leading to structural flexibility. The dependence of the propulsive efficiency on the geometry of the airframe for the ram compression and external combustion and expansion leads to a coupling between the aerodynamics, structural dynamics and the propulsion system which must be addressed by the flight control system.

An analytical model based on Newtonian Impact Theory[1-3] and aero/thermo analysis of the flow in a Scramjet-type propulsion system has been among the most commonly used for simulation and control design. The dynamics are strongly influenced by both propulsive and aerodynamic effects, and structural dynamics of the (assumed) elastic vehicle are accounted for using a lump-mass model. Using Lagrangian methods[4], a model has been obtained which captures the dynamics due to the rigid-body, elastic deformation, fluid flow, rotating machinery, wind, and a spherical rotating Earth. Force, moment, and elastic-deformation equations are derived, as well as appropriate kinematic equations. A model based on Compressible Flow Theory is under development[5] that captures the flexible structure, aerodynamic, and propulsion system coupling. This model will be described below, and will be used in this research for control design algorithm development and testing.

Study of the flight dynamics of HSV's has shown that the vehicles are nonlinear, time-varying, coupled, unstable, and non-minimum phase. Furthermore, initial simulations indicated very slow response to a reference command. The structural dynamics introduce further complications to the control problem, including modal uncertainty due to coupling effects, potentially time-varying modal frequencies, and the presence of structural modes with frequencies within the control bandwidth. Propulsive effects can be essentially viewed as disturbances to the flight control system. Note that elevator effects constitute an unstable zero dynamics that renders the overall system non-minimum phase.[*] If these effects can be canceled using throttle (possible if it produces significant direct lift at or forward of the CG and responds quickly) or by using additional control effectors such as a canard, then the overall non-minimum phase behavior will be reduced or eliminated.

Flight controller design methods for hypersonic and other elastic vehicles have been an important topic, and interest continues to grow. A robust control system design has been presented[6,7] that uses a genetic algorithm to search a design coefficient space. Each search point is evaluated using a Monte Carlo routine that estimates stability and performance robustness. Using a 0-1 scale for probability of the vehicle going unstable, the resulting controller reduced the likelihood of instability from 0.816 to 0.014 compared to open loop operation. Controllers based on the mixed-sensitivity H_∞ technique[8] have been presented that achieve good performance over a large flight envelope. The authors address concerns of instability inherent in the technique by ensuring that the frozen operation design points are chosen carefully. An output feedback technique[9] using a novel error observer has shown good performance in the presence of flexible modes. An examination of the flight dynamics of hypersonic air breathing vehicles[10] reveals the extensive coupling between flight-path and attitude dynamics in the hypersonic region. Additionally, this study demonstrates that propulsive performance varies with altitude, Mach number, and angle of attack. The presence of non-minimum phase characteristics of the lifting body design are addressed[11] by proposing an additional control surface. The presence of a canard that is ganged with the elevator can force the right-half plane transmission zero further to the right, allowing for increased freedom in control design in the form of increased controller bandwidth. A pseudo dynamic inversion (DI) controller is proposed[12] that uses an additional feedback loop to stabilize the zero dynamics. This avoids the right-half plane pole that DI would introduce in an attempt to cancel the non minimum phase zero. Another DI-based method uses a spline-interpolated lookup table[13] during simulation to calculate the force coefficients, and has shown promising results.

In the current research, the authors study the application of Trajectory Linearization Control[14-16] (TLC) to the HSV control problem. Nonlinear tracking and decoupling control using TLC is based on Differential Algebraic Spectral Theory (DAST), and can be viewed as the ideal gain-scheduling controller designed at every point on the flight trajectory. It is an analytical design that provides robustness by design (as opposed to worst-case optimal). It combines open-loop and closed-loop control, and is model based, thereby making maximal utilization of known vehicle properties. In addition, it is adaptive, using time-varying bandwidth (gain) to allow adaptation to modeling errors and uncertainties, disturbances, control saturations, and failures.

The inherent flexibility of the airframe is an especially vital consideration, and research in this area is very active as well. An online adaptive filtering technique[17] that can simultaneously identify multiple modes for flexible parameters has been introduced, although results are limited to widely-spaced frequencies. A procedure based on deeper understanding of acuator dynamics is suggested[18], and results in a less conservative design.

This paper describes the HSV models under study in Section II, and provides the theoretical background and practical application of TLC, including the controller design process for the rigid body HSV longitudinal dynamics model in Section III. A control allocation scheme is discussed in Section IV. Section V describes the current Matlab/SIMULINK implementation of TLC on the AFRL model, and the trim-testing and step response results are presented. Section VI concludes the paper with a summary of the main results.

II. Modeling

A. First-Principles Based Hypersonic Vehicle Model

Researchers at Wright Patterson Air Force Base (WPAFB) in Dayton, OH are developing a generic, hypersonic vehicle longitudinal dynamics model that takes into account structural, aerodynamic, and propulsion system coupling.[5] Compressible flow theory is used to determine the pressures acting on the vehicle, and oblique shock theory is used to determine the angle of the bow shock. The forces acting on the airframe are derived in the body axis as F_x and F_z, where the propulsion and aerodynamic forces and moment M_y are heavily coupled and are nonlinear functions of the state variables altitude h, velocity V_t, angle of attack α, and control variables elevator deflection δ_{e}, engine throttle (equivalence fuel ratio) δ_{th}, and the cowl door distance x_{d}. The model has been implemented in MATLAB, and will be treated as a black box.

B. Nonlinear Affine Rigid Body Model for TLC Design

Typical modern nonlinear flight control techniques employ the affine nonlinear state equation model

$$\dot{x} = f(x) + g(x)\mu$$

$$\eta = h(x) + d(x)\mu$$

where x is the state vector, μ is the control vector, and η is the output vector. The vector field f usually captures inertial and structural couplings, as well as aerodynamic and propulsion couplings of the state variables, while the vector field g represents effectiveness of the control effectors on the rate of change of the state variables.

In order to maximize the crosscutting capability of our design for scaling or alteration of the airframe, or migration to different airframes, we choose to seperate the inertial/structural dynamics from the aero/propulsive dynamics as

$$\dot{x} = f_1(x) + f_2(x) + g(x)\mu$$

where $f_1(x)$ captures the inertial/structural dynamics due to vehicle mass properties and strucural configuration that can be determined by analysis and testing, while $f_2(x)$ represents aerodynamic and propulsive forces and moments that are usually determined by CFD analysis, wind tunnel testing, and flight data. The control design will first use $f_2(x)$ as virtual controls to achieve desired motion, then realize the virtual control commands as a (static) control allocation design. To this end, and at the present stage, the longitudinal rigid body equations of motion in the stability frame is given by

$$\dot{h} = V_t \sin\gamma$$

$$\dot{\gamma} = \left(\frac{L}{m} - g\cos\gamma\right)\frac{1}{V_t}$$

$$\dot{V}_t = \frac{T}{m} - g\sin\gamma$$

$$\dot{\theta} = Q$$

$$\dot{Q} = \frac{1}{I_{yy}} M_y$$

where L is the total lift force, T is the net thrust force, and M_y is the total pitching moment. These variables will be used as virtual controls $L = \mu_1, T = \mu_2,\ M_y = \mu_3,$ and are decomposed into components

$$L = L_{\text{aero}} + L_{\text{prop}} + L_{\text{ctrl}}$$

$$T = -D_{\text{aero}} + T_{\text{prop}} - D_{\text{ctrl}}$$

$$M_y = M_{y,\text{aero}} + M_{y,\text{prop}}$$

The physical constant parameters are given by:

$m = 300$ slug, $g = 32.17$ ft/s^2, $Re = 2.093 \times 10^7$, $I_{yy} = 5 \times 10^5$slug-ft^2.

With the state, virtual control input, and output variables defined as given in the nomenclature, the state and output equations can be written as:

$$\begin{bmatrix} \dot{h} \\ \dot{\gamma} \\ \dot{V}_t \\ \dot{\theta} \\ \dot{Q} \end{bmatrix} = \begin{bmatrix} V_t \sin\gamma \\ -g\,\frac{1}{V_t}\cos\gamma \\ -g\sin\gamma \\ Q \\ 0 \end{bmatrix} + \begin{bmatrix} 0 & 0 & 0 \\ \frac{1}{m}\frac{1}{V_t} & 0 & 0 \\ 0 & \frac{1}{m} & 0 \\ 0 & 0 & 0 \\ 0 & 0 & \frac{1}{I_{yy}} \end{bmatrix} \begin{bmatrix} L \\ T \\ M_y \end{bmatrix}$$
$$= f(x) + g(x)\mu$$

$$\begin{bmatrix} L \\ T \\ M_y \end{bmatrix} = \begin{bmatrix} L_{\text{prop}} + L_{\text{aero}} + L_{\text{ctrl}} \\ T_{\text{prop}} - D_{\text{aero}} - D_{\text{ctrl}} \\ M_{y,\text{prop}} + M_{y,\text{aero}} \end{bmatrix} = b(\delta, \alpha, V_t)$$

$$\begin{bmatrix} \eta_1 \\ \eta_2 \end{bmatrix} = \begin{bmatrix} \gamma \\ V_t \end{bmatrix} = h(x).$$

Not$e$ that in this simplified case h is neither regulated nor measured. However, the altitude will have an effect on the lift, drag, propulsion, and control forces and moments due to the variations in density and temperature, and will be included in the design. For autonomous flight, the regulated variables can be the altitude and down range trajectories. In that case, flight path angle and velocity become intermediate variables.

C. Nonlinear Affine Virtual Control and Control Effector Model

This study assumes an affine, nonlinear actuator model for virutal control and control effectors in the form of

$$p(x) = p_{\text{trim}} + \tilde{p}$$

where $p_{\text{trim}} = p(x_{\text{trim}})$ is the nominal value of p at the trimmed (equilibrium) flight condition x_{trim}, and $\tilde{p}$ is the perturbation from the nominal which will be approximated by

$$\tilde{p} = \left.\frac{\partial p}{\partial x}\right|_{x_{\text{trim}}} \tilde{x}$$

where $\tilde{x}$ is the perturbation of the flight condition from x_{trim}. The forces and pitch moment are given by

$$L_{\text{aero}} = C_{L_\alpha}\tilde{\alpha} + L_{\text{aero,trim}}$$

$$D_{\text{aero}} = C_{D_\alpha}\tilde{\alpha} + D_{\text{aero,trim}}$$

$$L_{\text{ctrl}} = C_{L_{\delta e}}\tilde{\delta}_e + L_{\text{ctrl,trim}}$$

$$D_{\text{ctrl}} = C_{D_{\delta e}}\tilde{\delta}_e + D_{\text{ctrl,trim}}$$

$$F_{\text{prop}} = C_{\delta_{\text{th}}}\tilde{\delta}_{\text{th}} + F_{\text{prop,trim}}$$

$$L_{\text{prop}} = \left(\tilde{F}_{\text{prop}} + F_{\text{prop,trim}}\right)\sin\alpha \simeq \tilde{F}_{\text{prop}}\sin\alpha_{\text{trim}} + F_{\text{prop,trim}}\sin\alpha_{\text{trim}}$$

$$T_{\text{prop}} = \left(\tilde{F}_{\text{prop}} + F_{\text{prop,trim}}\right)\cos\alpha \simeq \tilde{F}_{\text{prop}}\cos\alpha_{\text{trim}} + F_{\text{prop,trim}}\cos\alpha_{\text{trim}}$$

$$M_y = C_{\delta e}\tilde{\delta}_e + M_{y,\text{trim}}$$

Thus

$$\tilde{L} = C_{\delta th}\tilde{\delta}_{\text{th}}\sin\alpha_{\text{trim}} + C_{L_\alpha}\tilde{\alpha} + C_{L_{\delta e}}\tilde{\delta}_e$$

$$\tilde{T} = C_{\delta_{th}}\tilde{\delta}_{\text{th}}\cos\alpha_{\text{trim}} - C_{D_\alpha}\tilde{\alpha} - C_{D_{\delta e}}\tilde{\delta}_e$$

$$\tilde{M}_y = C_{M\delta_{\text{th}}}\tilde{\delta}_{\text{th}} + C_{M_\alpha}\tilde{\alpha} + C_{M_{\delta e}}\tilde{\delta}_e$$

where

$$\tilde{L} = L - L_{\text{trim}} = L - F_{\text{prop,trim}}\sin\alpha_{\text{trim}} - L_{\text{aero,trim}} - L_{\text{ctrl,trim}}$$

$$\tilde{T} = T - T_{\text{trim}} = T - F_{\text{prop,trim}}\cos\alpha_{\text{trim}} + D_{\text{aero,trim}} + D_{\text{ctrl,trim}}$$

$$\tilde{M}_y = M_y - M_{y,\text{trim}}$$

$$\tilde{\alpha} = \alpha - \alpha_{\text{trim}}$$

$$\tilde{\delta}_e = \delta_{\text{e}} - \delta_{\text{e,trim}}$$

$$\tilde{\delta}_{\text{th}} = \delta_{\text{th}} - \delta_{\text{th,trim}}$$

In this case, the parameters of the model are given by

$$C_{\delta th}(V_{t,\text{trim}}, h_{\text{trim}}) = \left.\frac{\partial F_{\text{prop}}}{\partial \delta_{\text{th}}}\right|_{V_{t,\text{trim}}, h_{\text{trim}}}$$

$$C_{M_{\delta\text{th}}}(V_{t,\text{trim}}, h_{\text{trim}}) = \left.\frac{\partial M_y}{\partial \delta_{\text{th}}}\right|_{V_{t,\text{trim}}, h_{\text{trim}}}$$

$$C_{L_\alpha}(V_{t,\text{trim}}, h_{\text{trim}}) = \left.\frac{\partial L_{\text{aero}}}{\partial \alpha}\right|_{V_{t,\text{trim}}, h_{\text{trim}}}$$

$$C_{D_\alpha}(V_{t,\text{trim}}, h_{\text{trim}}) = \left.\frac{\partial D_{\text{aero}}}{\partial \alpha}\right|_{V_{t,\text{trim}}, h_{\text{trim}}}$$

$$C_{M\alpha}(V_{t,\text{trim}}, h_{\text{trim}}) = \left.\frac{\partial M_y}{\partial \alpha}\right|_{V_{t,\text{trim}}, h_{\text{trim}}}$$

$$C_{L_{\delta e}}(V_{t,\text{trim}}, h_{\text{trim}}) = \left.\frac{\partial L_{\text{aero}}}{\partial \delta_{\text{e}}}\right|_{V_{t,\text{trim}}, h_{\text{trim}}}$$

$$C_{D_{\delta e}}(V_{t,\text{trim}}, h_{\text{trim}}) = \left.\frac{\partial D_{\text{aero}}}{\partial \delta_{\text{e}}}\right|_{V_{t,\text{trim}}, h_{\text{trim}}}$$

$$C_{M_{\delta \text{e}}}(V_{t,\text{trim}}, h_{\text{trim}}) = \left.\frac{\partial M_y}{\partial \delta_{\text{e}}}\right|_{V_{t,\text{trim}}, h_{\text{trim}}}$$

where the trim values and derivatives are obtained from the AFRL Model by performing a two-dimensional optimization at multiple operating points based on velocity and altitude.

III. Trajectory Linearization Controller Design and Simulation Implementation

A. Trajectory Linearization Control (TLC)

TLC provides robust stability and performance without interpolation of controller gains, and eliminates costly controller redesigns due to minor airframe alteration. Controller gains for the commanded torque are computed symbolically based on the theoretical derivations and are applicable to any feasible trajectories and airframes with known mass properties. Therefore the design is scalable and mission adaptable. Additional features include the use of correct time-varying eigenvalue stability theory, and automated design using symbolic toolbox script. There is no interpolating for gain-scheduling needed, since the method provides 'ideal' gain-scheduling at every point along guidance trajectory.

Figure 1 shows a conceptual block diagram of the TLC method. A so-called pseudo-inverse is obtained for the nonlinear plant model to calculate the open-loop nominal control. The tracking error is then driven toward zero exponentially using a linear time-varying (LTV) tracking error regulator.

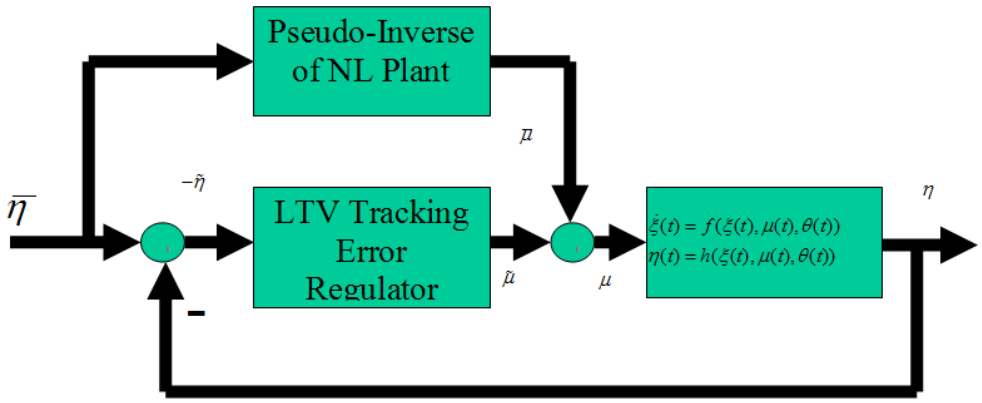

Figure 1. Conceptual Configuration Trajectory Linearization Control.

B. TLC Guidance and Attitude Controller Design

The control design method has been applied to the affine, nonlinear, rigid-body vehicle longitudinal model with a simplified linear control allocation. The design will be carried out for a slow translational (guidance) loop and a fast rotational (attitude) loop based on time-scale separation (singular perturbation principle).

1. The Guidance (Translational Motion) Loop

The reference command inputs are the commanded flight path angle γ_{com} and the commanded velocity $V_{t_{\text{com}}}$. The (virtual) control effector inputs to the guidance loop are chosen to be the throttle δ_{th} and the commanded angle of attack α_{com}. The outputs are the same as the overall system. The effects of the elevator deflection δ_e are treated as a disturbance that is ignored in the controller design. The guidance loop equations of motion are given by

$$\begin{aligned}\begin{bmatrix}\dot{\gamma}\\ \dot{V}_t\end{bmatrix} &= \begin{bmatrix}-g\,\frac{1}{V_t}\cos\gamma\\ -g\sin\gamma\end{bmatrix} + \begin{bmatrix}\frac{1}{m}\frac{1}{V_t} & 0\\ 0 & \frac{1}{m}\end{bmatrix}\begin{bmatrix}L\\ T\end{bmatrix}\\ &= f_{\text{gl}}(x_{\text{gl}}) + g_{\text{gl}}(x_{\text{gl}})\mu_{\text{gl}}\end{aligned}$$

$$\begin{bmatrix}\eta_1\\ \eta_2\end{bmatrix} = \begin{bmatrix}\gamma\\ V_t\end{bmatrix} = h(x)$$

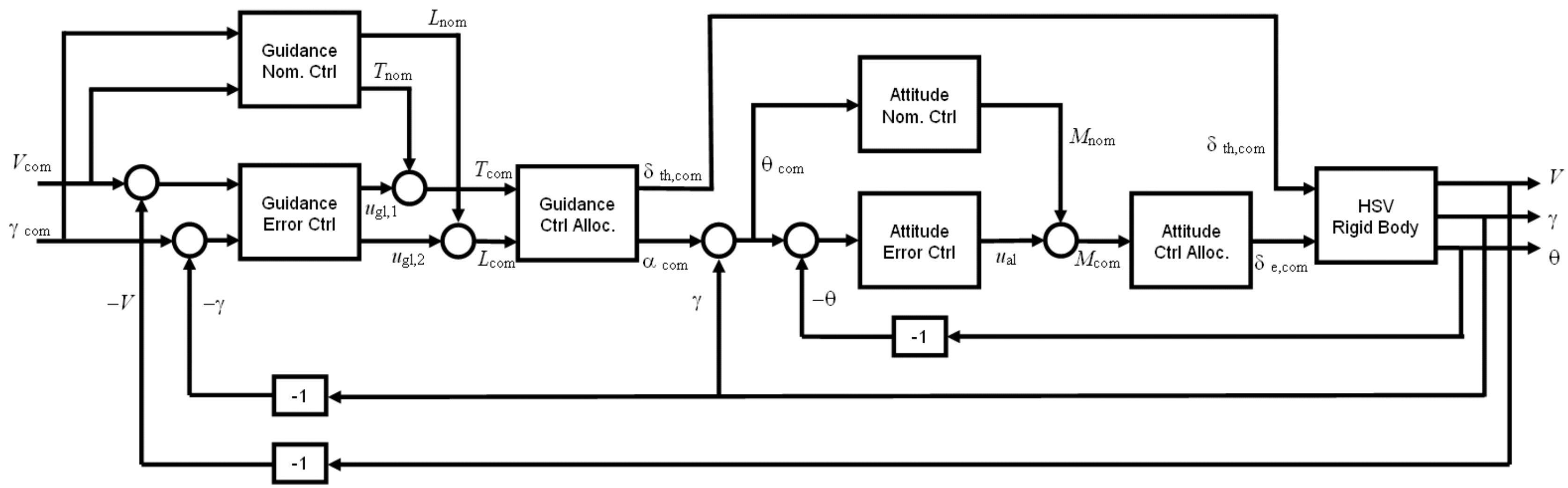

Figure 2. HSV TLC Controller Configuration

i. Nominal Guidance Controller Design:

Since $h(x)$ is independent of the input μ_{gl}, the relative degree is greater than zero. Taking the time derivative of η_1 once yields

$$\dot{\eta}_1 = \dot{\gamma} = -g\,\frac{1}{V_t}\cos\gamma + \frac{1}{m}\frac{1}{V_t}L$$
$$\dot{\eta}_2 = \dot{V}_t = -g\sin\gamma + \frac{1}{m}T$$

Thus the system has a vector relative degree $[1\ 1]$. The inverse mapping from $\dot{\overline{\eta}}$ to $\overline{\mu}_{\text{gl}}$ is given by

$$\overline{L} = m\big(\,\overline{Q}\,\dot{\overline{\eta}}_1 + g\cos\overline{\gamma}\,\big)$$
$$\overline{T} = m(\dot{\overline{\eta}}_2 + g\sin\overline{\gamma}\,)$$

The first-order pseudo-differentiators are designed by

$$\dot{\widehat{\overline{\eta}}}_i = \omega_{\text{diff},i}(\overline{\eta}_i - \widehat{\overline{\eta}}_i), \qquad i = 1,2$$

Note that $\widehat{\overline{\eta}}_1 = \widehat{\overline{\gamma}}$, $\widehat{\overline{\eta}}_2 = \widehat{\overline{V}}_t$. The state equation of the pseudo dynamic inverse of the plant is then given by

$$\begin{bmatrix} \dot{\widehat{\overline{\gamma}}} \\ \dot{\widehat{\overline{V}}}_t \end{bmatrix} = \begin{bmatrix} -\omega_{\text{diff},1}\widehat{\overline{\gamma}}_2 \\ -\omega_{\text{diff},2}\widehat{\overline{V}}_t \end{bmatrix} + \begin{bmatrix} \omega_{\text{diff},1} & 0 \\ 0 & \omega_{\text{diff},2} \end{bmatrix} \begin{bmatrix} \overline{\eta}_1 \\ \overline{\eta}_2 \end{bmatrix}$$
$$= \Phi_{\text{gl}}(\widehat{\overline{x}}_{\text{gl}}) + \Gamma_{\text{gl}}(\widehat{\overline{x}}_{\text{gl}})\,\overline{\eta}$$

$$\begin{bmatrix} \overline{L} \\ \overline{T} \end{bmatrix} = \begin{bmatrix} -m\Big(\widehat{\overline{V}}_t\omega_{\text{diff},1}\widehat{\overline{\gamma}} - g\cos\widehat{\overline{\gamma}}\Big) \\ -m\Big(\omega_{\text{diff},2}\widehat{\overline{V}}_t - g\sin\widehat{\overline{\gamma}}\Big) \end{bmatrix} + \begin{bmatrix} m\widehat{\overline{V}}_t\omega_{\text{diff},1} & 0 \\ 0 & m\omega_{\text{diff},2} \end{bmatrix} \begin{bmatrix} \overline{\eta}_1 \\ \overline{\eta}_2 \end{bmatrix}$$
$$= \Psi_{\text{gl}}(\widehat{\overline{x}}_{\text{gl}}) + \Omega_{\text{gl}}(\widehat{\overline{x}}_{\text{gl}})\,\overline{\eta}$$

Clearly, the pseudo-inverse is globally exponentially stable. It is noted that in unaccelerated cruise flight, the nominal thrust $\overline{T} = 0$. This is because the aerodynamic drag force is not included in the plant model. Rather, it is included in the guidance control allocation. Thus, $\overline{T} = 0$ does not mean the throttle $\delta_{\text{th}} = 0$. In fact $\delta_{\text{th}} = \delta_{\text{th,trim}}$, which generates the thrust that cancels out the aerodynamic drag force.

ii. Guidance Tracking Error Stabilization Controller Design:

Define the (augmented) tracking error variables by

$$\begin{bmatrix} \tilde{\gamma}_{\text{int}}(t) \\ \tilde{\gamma}_2(t) \\ \tilde{V}_{\text{int}}(t) \\ \tilde{V}(t) \end{bmatrix} = \begin{bmatrix} \int_0^t(\gamma(\tau) - \overline{\gamma}\,(\tau))d\tau \\ \gamma(t) - \overline{\gamma}\,(t) \\ \int_0^t\big(V_t(\tau) - \overline{Q}\,(\tau)\big)d\tau \\ V_t(t) - \overline{Q}\,(t) \end{bmatrix}$$

$$\begin{bmatrix} \tilde{L}(t) \\ \tilde{T}(t) \end{bmatrix} = \begin{bmatrix} L(t) - \overline{L}\,(t) \\ T(t) - \overline{T}\,(t) \end{bmatrix}$$

$$\begin{bmatrix} \tilde{\eta}_1(t) \\ \tilde{\eta}_2(t) \end{bmatrix} = \begin{bmatrix} \eta_1(t) - \overline{\eta}_1(t) \\ \eta_2(t) - \overline{\eta}_2(t) \end{bmatrix}$$

Then the tracking error dynamics is given by

$$\begin{aligned} \begin{bmatrix} \dot{\tilde{\gamma}}_{\text{int}} \\ \dot{\tilde{\gamma}} \\ \dot{\tilde{V}}_{t_{\text{int}}} \\ \dot{\tilde{V}}_t \end{bmatrix} &= \begin{bmatrix} \tilde{\gamma}_2 \\ -g\left[\frac{1}{\tilde{\xi}_3+\overline{Q}(t)}\cos(\tilde{\gamma}+\overline{\gamma}(t))\right] \\ \tilde{V}_t \\ -g\left[\sin(\tilde{\gamma}+\overline{\gamma}(t)) + \sin\overline{\gamma}(t)\right] \end{bmatrix} + \begin{bmatrix} 0 \\ \frac{1}{m}\left[\frac{1}{\tilde{V}_t+\overline{Q}}\left(\tilde{L}+\overline{L}(t)\right) - \frac{1}{\overline{Q}}\overline{L}(t)\right] \\ 0 \\ \frac{1}{m}\tilde{T}_2 \end{bmatrix} \\ &= \tilde{f}_{\text{gl}}(\tilde{x}_{\text{gl}}, \overline{x}_{\text{gl}}(t)) + \tilde{g}_{\text{gl}}\left(\tilde{x}_{\text{gl}}, \tilde{\mu}_{\text{gl}}, \overline{x}_{\text{gl}}(t), \overline{\mu}_{\text{gl}}(t)\right) \end{aligned}$$

$$\begin{bmatrix} \tilde{\eta}_1 \\ \tilde{\eta}_2 \end{bmatrix} = \begin{bmatrix} \tilde{\gamma} \\ \tilde{V}_t \end{bmatrix} = \tilde{h}(\tilde{x}_{\text{gl}}, \overline{x}_{\text{gl}}(t))$$

Linearization along the nominal trajectory yields the linearized tracking error dynamics

$$\begin{aligned} \dot{x}_{\text{gl}} &= A_{\text{gl}}(t)x_{\text{gl}} + B_{\text{gl}}(t)u_{\text{gl}} \\ y_{\text{gl}} &= C_{\text{gl}}(t)x_{\text{gl}} + D_{\text{gl}}(t)u_{\text{gl}} \end{aligned}$$

where

$$A_{\text{gl}}(t) = \left.\frac{\partial f_{\text{gl}}}{\partial x_{\text{gl}}}\right|_{\overline{x}_{\text{gl}},\overline{\mu}_{\text{gl}}} = \begin{bmatrix} 0 & 1 & 0 & 0 \\ 0 & g\,\frac{1}{\overline{Q}(t)}\sin\overline{\gamma}(t) & 0 & g\,\frac{1}{\overline{Q}^2(t)}\cos\overline{\gamma}(t) \\ 0 & 0 & 0 & 1 \\ 0 & -g\cos\overline{\gamma}(t) & 0 & 0 \end{bmatrix}$$

$$B_{\text{gl}}(t) = \left.\frac{\partial f_{\text{gl}}}{\partial \mu_{\text{gl}}}\right|_{\overline{x}_{\text{gl}},\overline{\mu}_{\text{gl}}} = \begin{bmatrix} 0 & 0 \\ \frac{1}{m}\frac{1}{\overline{Q}(t)} & 0 \\ 0 & 0 \\ 0 & \frac{1}{m} \end{bmatrix}$$

$$C_{\text{gl}}(t) = \left.\frac{\partial h_{\text{gl}}}{\partial x_{\text{gl}}}\right|_{\overline{x}_{\text{gl}},\overline{\mu}_{\text{gl}}} = \begin{bmatrix} 0 & 1 & 0 & 0 \\ 0 & 0 & 0 & 1 \end{bmatrix}$$

Let the desired closed-guidance-loop (CGL) tracking error dynamics be given by

$$A_{\text{cgl}}(t) = \begin{bmatrix} 0 & 1 & 0 & 0 \\ -a_{111}(t) & -a_{112}(t) & 0 & 0 \\ 0 & 0 & 0 & 1 \\ 0 & 0 & -a_{121}(t) & -a_{122}(t) \end{bmatrix}$$

where

$$\begin{aligned} a_{1i1}(t) &= \omega_{1i}^2(t) \qquad\qquad i = 1,2 \\ a_{1i2}(t) &= 2\zeta_{1i}\omega_{1i}(t) - \frac{\dot{\omega}_{1i}(t)}{\omega_{1i}(t)} \end{aligned}$$

Design a proportional-integral (PI) state feedback control law

$$\begin{aligned} u_{\text{gl}} &= K_{\text{cgl}}(t)x_{\text{gl}} \\ &= K_{\text{P,cgl}}(t)\begin{bmatrix} x_2 \\ x_4 \end{bmatrix} + K_{\text{I,cgl}}(t)\begin{bmatrix} x_1 \\ x_3 \end{bmatrix} \end{aligned}$$

where the controller gain matrix is found from

$$K_{\text{cgl}}(t) = [R_{\text{gl}} B_{\text{gl}}(t)]^{-1} R_{\text{gl}} [A_{\text{cgl}}(t) - A_{\text{gl}}(t)]$$
$$= \begin{bmatrix} m\overline{Q}\,(t) & 0 \\ 0 & m \end{bmatrix} \begin{bmatrix} -a_{111}(t) & -a_{112}(t) + g\,\frac{1}{\overline{Q}(t)}\sin\overline{\gamma}\,(t) & 0 & g\,\frac{1}{\overline{Q}^2(t)}\cos\overline{\gamma}\,(t) \\ 0 & g\cos\overline{\gamma}\,(t) & -a_{121}(t) & -a_{122}(t) \end{bmatrix}$$

where

$$R_{\text{gl}} = \begin{bmatrix} 0 & 1 & 0 & 0 \\ 0 & 0 & 0 & 1 \end{bmatrix}$$

iii. Guidance Loop Control Allocation

The overall guidance loop virtual control is given by

$$\begin{bmatrix} L \\ T \end{bmatrix} = \begin{bmatrix} \overline{\mu}_1 \\ \overline{\mu}_2 \end{bmatrix} + \begin{bmatrix} u_1 \\ u_2 \end{bmatrix}$$

The guidance loop control effectors are chosen to be the fuel equivalence ratio (throttle) δ_{th} and the angle of attack α (in degrees).

B. The Attitude (Rotational Motion) Loop

The reference command is the commanded angle of attack α_{com} generated by the guidance loop. However, the attitude loop state variables are chosen to be the Euler pitch angle θ and the body pitch rate Q, which are also measured for state feedback. Thus, the commanded angle of attack is achieved via the commanded pitch angle $\theta_{\text{com}} = \alpha_{\text{com}} + \gamma$. The virtual control input is chosen to be the pitch moment $M_y = M_y$. The regulated output for the attitude loop is the pitch angle θ. The equations of motion for the attitude loop are given by

$$\begin{bmatrix} \dot{\theta} \\ \dot{Q} \end{bmatrix} = \begin{bmatrix} Q \\ 0 \end{bmatrix} + \begin{bmatrix} 0 \\ \frac{1}{I_{yy}} \end{bmatrix} [\, M_y \,]$$
$$= f_{\text{al}}(x_{\text{al}}) + g_{\text{al}}(x)\mu_{\text{al}}$$
$$[\eta_3] = \theta = h_{\text{al}}(x_{\text{al}})$$

i. Nominal Attitude Control Design

The attitude EOM is a linear system with relative degree 2. Thus the inverse mapping from $\dot{\overline{\eta}}_3$ to $\overline{\mu}_3$ is given by

$$\overline{\mu}_3 = I_{yy}\ddot{\overline{\eta}}_3$$

The second-order pseudo-differentiators are designed by:

$$\ddot{\widehat{\overline{\eta}}}_3 = \omega_{\text{diff},3}^2 \overline{\eta}_i - \left(2\,\zeta_{\text{diff},3}\,\omega_{\text{diff},3} \dot{\widehat{\overline{\eta}}}_3 + \omega_{\text{diff},3}^2 \widehat{\overline{\eta}}_3\right)$$

Note that $\dot{\widehat{\overline{\eta}}}_3 = \widehat{\overline{Q}}$, $\widehat{\overline{\eta}}_3 = \widehat{\overline{\theta}}$. The state equation of the pseudo dynamic inverse of the plant is then given by

$$\begin{bmatrix} \dot{\widehat{\overline{\theta}}} \\ \dot{\widehat{\overline{Q}}} \end{bmatrix} = \begin{bmatrix} 0 & 1 \\ -\omega_{\text{diff},3}^2 & -2\,\zeta_{\text{diff},3}\,\omega_{\text{diff},3} \end{bmatrix} \begin{bmatrix} \widehat{\overline{\theta}} \\ \widehat{\overline{Q}} \end{bmatrix} + \begin{bmatrix} 0 \\ \omega_{\text{diff},3}^2 \end{bmatrix} [\, \overline{\eta}_3 \,]$$
$$= \Phi_{\text{al}}(\widehat{\overline{\xi}}_{\text{al}}) + \Gamma_{\text{al}}(\widehat{\overline{\xi}}_{\text{al}})\,\overline{\eta}$$

$$
\begin{aligned}
[\,\overline{\mu}_3\,] &= \left[-I_{yy}\left(2\,\zeta_{\text{diff},3}\,\omega_{\text{diff},3}\widehat{\overline{Q}} + \omega^2_{\text{diff},3}\widehat{\overline{\theta}}\right)\right] + \left[\,I_{yy}\omega^2_{\text{diff},3}\,\overline{\eta}_3\right] \\
&= \Psi_{\text{al}}(\widehat{\overline{x}}_{\text{al}}) + \Omega_{\text{al}}(\widehat{\overline{x}}_{\text{al}})\,\overline{\eta}_3
\end{aligned}
$$

Clearly, the pseudo-inverse is globally exponentially stable.

<u>ii. Attitude Tracking Error Stabilization Controller Design:</u>

Define the (augmented) tracking error variables by

$$
\begin{bmatrix} \tilde{\theta}_{\text{int}}(t) \\ \tilde{\theta}(t) \\ \tilde{V}_t(t) \end{bmatrix} = \begin{bmatrix} \int_0^t \big(\theta(\tau) - \overline{\theta}\,(\tau)\big)d\tau \\ \theta(t) - \overline{\theta}\,(t) \\ V_t(t) - \overline{V}_t(t) \end{bmatrix}
$$

$$
\left[\,\tilde{M}_y(t)\,\right] = \left[\,M_y(t) - \overline{M}_y(t)\,\right]
$$

$$
[\,\tilde{\eta}_3(t)\,] = [\,\eta_3(t) - \overline{\eta}_3(t)\,]
$$

Then the tracking error dynamics is given by

$$
\begin{aligned}
\begin{bmatrix} \dot{\tilde{\theta}}_{\text{int}} \\ \tilde{\theta} \\ \dot{\tilde{V}}_t \end{bmatrix} &= \begin{bmatrix} \tilde{\theta} \\ \tilde{Q} \\ 0 \end{bmatrix} + \begin{bmatrix} 0 \\ 0 \\ \frac{1}{I_{yy}} \end{bmatrix} [\,\tilde{M}_y\,] \\
&= \tilde{f}_{\text{al}}(\tilde{x}_{\text{al}}, \overline{x}_{\text{al}}(t)) + \tilde{g}_{\text{al}}(\tilde{x}_{\text{al}}, \tilde{\mu}_{\text{al}}, \overline{x}_{\text{al}}(t), \overline{\mu}_{\text{al}}(t))
\end{aligned}
$$

$$
[\,\tilde{\eta}_3\,] = \left[\,\tilde{\theta}\,\right] = \tilde{h}_{\text{al}}(\tilde{x}_{\text{al}}, \overline{x}_{\text{al}}(t))
$$

Linearization along the nominal trajectory yields the linearized tracking error dynamics

$$
\begin{aligned}
\dot{x}_{\text{al}} &= A_{\text{al}}(t)x_{\text{al}} + B_{\text{al}}(t)u_{\text{al}} \\
y_{\text{al}} &= C_{\text{al}}(t)x_{\text{al}} + D_{\text{al}}(t)u_{\text{al}}
\end{aligned}
$$

where

$$
\begin{aligned}
A_{\text{al}}(t) &= \left.\frac{\partial f_{\text{al}}}{\partial x_{\text{al}}}\right|_{\overline{x}_{\text{al}},\overline{\mu}_{\text{al}}} = \begin{bmatrix} 0 & 1 & 0 \\ 0 & 0 & 1 \\ 0 & 0 & 0 \end{bmatrix} \\
B_{\text{al}}(t) &= \left.\frac{\partial f_{\text{al}}}{\partial \mu_{\text{al}}}\right|_{\overline{x}_{\text{al}},\overline{\mu}_{\text{al}}} = \begin{bmatrix} 0 \\ 0 \\ \frac{1}{I_{yy}} \end{bmatrix} \\
C_{\text{al}}(t) &= \left.\frac{\partial h_{\text{al}}}{\partial x_{\text{al}}}\right|_{\overline{x}_{\text{al}},\overline{\mu}_{\text{al}}} = \begin{bmatrix} 0 & 1 & 0 \end{bmatrix}
\end{aligned}
$$

Let the desired closed-attitude-loop tracking error dynamics be given by

$$
A_{\text{cal}}(t) = \begin{bmatrix} 0 & 1 & 0 \\ 0 & 0 & 1 \\ -a_{21}(t) & -a_{22}(t) & -a_{23}(t) \end{bmatrix}
$$

where for constant closed-loop eigenvalues ρ_1, ρ_2, ρ_3,

$$
\begin{aligned}
a_{21}(t) &= -\rho_1\rho_2\rho_3 \\
a_{22}(t) &= \rho_1\rho_2 + \rho_2\rho_3 + \rho_3\rho_1 \\
a_{22}(t) &= -(\rho_1 + \rho_2 + \rho_3).
\end{aligned}
$$

The proportional-integral (PI) state feedback control law is designed by:

$$u_{\text{al}} = K_{\text{cal}}(t)x_{\text{al}}$$

where the controller gain matrix is found from

$$
\begin{aligned}
K_{\text{cal}}(t) &= [R_{\text{al}}B_{\text{al}}(t)]^{-1}R_{\text{al}}[A_{\text{cal}}(t) - A_{\text{al}}(t)] \\
&= [I_{yy}]\begin{bmatrix} -a_{21}(t) & -a_{22}(t) & -a_{23}(t) \end{bmatrix}
\end{aligned}
$$

where

$$R_{\text{al}} = \begin{bmatrix} 0 & 0 & 1 \end{bmatrix}$$

<u>iii. Attitude Loop Control Allocation</u>

The overall attitude loop control is given by

$$\begin{bmatrix} M_y \end{bmatrix} = \begin{bmatrix} \bar{M}_y \end{bmatrix} + \begin{bmatrix} u_{\text{al}} \end{bmatrix}$$

The allocation will be designed together with the guidance loop in the next section.

IV. Control Allocation Design

Inverse Jacobian Approach

The control allocation is redesigned by inverting the equations for $\tilde{L}$, T, and $\tilde{M}$. Define the Jacobian matrix as

$$
J(V_{t,\text{trim}}, h_{\text{trim}}) = \begin{bmatrix}
\left.\frac{\partial F_{\text{prop}}}{\partial \delta_{\text{th}}}\right|_{V_{t,\text{trim}},h_{\text{trim}}} \sin\alpha_{\text{trim}} & \left.\frac{\partial L_{\text{aero}}}{\partial \alpha}\right|_{V_{t,\text{trim}},h_{\text{trim}}} & \left.\frac{\partial L_{\text{aero}}}{\partial \delta_{\text{e}}}\right|_{V_{t,\text{trim}},h_{\text{trim}}} \\
\left.\frac{\partial F_{\text{prop}}}{\partial \delta_{\text{th}}}\right|_{V_{t,\text{trim}},h_{\text{trim}}} \cos\alpha_{\text{trim}} & -\left.\frac{\partial D_{\text{aero}}}{\partial \alpha}\right|_{V_{t,\text{trim}},h_{\text{trim}}} & -\left.\frac{\partial D_{\text{aero}}}{\partial \delta_{\text{e}}}\right|_{V_{t,\text{trim}},h_{\text{trim}}} \\
\left.\frac{\partial M_y}{\partial \delta_{\text{th}}}\right|_{V_{t,\text{trim}},h_{\text{trim}}} & \left.\frac{\partial M_y}{\partial \alpha}\right|_{V_{t,\text{trim}},h_{\text{trim}}} & \left.\frac{\partial M_y}{\partial \delta_{\text{e}}}\right|_{V_{t,\text{trim}},h_{\text{trim}}}
\end{bmatrix}
$$

We have

$$
\begin{bmatrix} L \\ T \\ M \end{bmatrix} = \begin{bmatrix} L_{\text{trim}} \\ T_{\text{trim}} \\ M_{\text{trim}} \end{bmatrix} + J_{\text{trim}} \begin{bmatrix} \tilde{\delta}_{\text{th}} \\ \tilde{\alpha} \\ \tilde{\delta}_e \end{bmatrix}.
$$

where

$$L_{\text{trim}} = T_{\text{prop,trim}} \sin\alpha_{\text{trim}} + L_{\text{aero,trim}} + L_{\text{ctrl,trim}}$$

$$T_{\text{trim}} = T_{\text{prop,trim}} \cos\alpha_{\text{trim}} - D_{\text{aero,trim}} - D_{\text{ctrl,trim}}$$

Assuming the Jacobian is nonsingular, we have

$$
\begin{bmatrix} \tilde{\delta}_{\text{th}} \\ \tilde{\alpha} \\ \tilde{\delta}_e \end{bmatrix} = J_{\text{trim}}^{-1} \begin{bmatrix} \tilde{L} \\ \tilde{T} \\ \tilde{M} \end{bmatrix}
$$

$$\begin{bmatrix} \delta_{\text{th}} \\ \alpha \\ \delta_{\text{e}} \end{bmatrix} \simeq \begin{bmatrix} \delta_{\text{th,trim}} \\ \alpha_{\text{trim}} \\ \delta_{\text{e,trim}} \end{bmatrix} + \begin{bmatrix} \tilde{\delta}_{\text{th}} \\ \tilde{\alpha} \\ \tilde{\delta}_e \end{bmatrix} = \begin{bmatrix} \delta_{\text{th,trim}} \\ \alpha_{\text{trim}} \\ \delta_{\text{e,trim}} \end{bmatrix} + J_{\text{trim}}^{-1} \begin{bmatrix} \tilde{L} \\ \tilde{T} \\ \tilde{M} \end{bmatrix}$$

To facilitate the initial control allocation design, we use the inverse Jacobian of the following simplified Jacobian matrix that allows the control allocation to be decoupled into the guidance tracking loop and attitude control tracking loop, and to circumvent the non-minimum phase effects of the lift due to the elevator that would likely lead to instability.

$$\widehat{J}(V_{t,\text{trim}}, h_{\text{trim}}) = \begin{bmatrix} \left.\frac{\partial T_{\text{prop}}}{\partial \delta_{\text{th}}}\right|_{V_{t,\text{trim}}, h_{\text{trim}}} \sin\alpha & \left.\frac{\partial L_{\text{aero}}}{\partial \alpha}\right|_{V_{t,\text{trim}}, h_{\text{trim}}} & 0 \\ \left.\frac{\partial T_{\text{prop}}}{\partial \delta_{\text{th}}}\right|_{V_{t,\text{trim}}, h_{\text{trim}}} \cos\alpha & -\left.\frac{\partial D_{\text{aero}}}{\partial \alpha}\right|_{V_{t,\text{trim}}, h_{\text{trim}}} & 0 \\ 0 & 0 & \left.\frac{\partial M_y}{\partial \delta_{\text{e}}}\right|_{V_{t,\text{trim}}, h_{\text{trim}}} \end{bmatrix}$$

Control Allocation Implementation

Lookup Tables

As a first step to accommodate varying flight conditions, a lookup table is formed that contains trim values for lift, thrust, moment, and effector configurations based on velocity and altitude. This approach gives good results and will be used a baseline performance. However, use of tables requires significant onboard data storage. For a large flight envelope, this may be cumbersome.

Curve Fitting

An alternate method of implementing the control allocation design above is to perform curve fits to obtain analytic expressions for the effector settings. Using Gaussian elimination, the data obtained for the lookup tables are fitted to the expressions of the form

$$\delta_i = c_1 M_o + c_2 M_o^2 + c_3 M_o^3 + c_4 h + c_5 h^2 + c_6,$$

and the tables are replaced with functions defined by these expressions. In the next section, simulation results are presented that utilize these fits for computation of effector settings. It is noted that, while curve fitting methods reduce the amount of onboard data storage, they do increase the computation time.

V. Simulation Implementation and Results

AFRL Rigid-Body Longitudinal Vehicle Model

In the current work, the affine model has been replaced by the rigid-body AFRL model. The TLC design used above is applied directly and preliminary results using the curve fitted allocation parameters are presented. The controller designed for affine model is used to perform trim and step response tests.

Trim testing result

In the initial simulation, the commanded trajectory is trimmed flight at Mach 8.0 and 85, 000 ft. Figures 4-11 show that the vehicle trims successfully within 100s.

Step response testing result

As shown in figures 12-23, a increase in velocity of 500 ft/s is commanded at $t = 100$s. It is seen that the controller designed for the affine model performs well on the nonlinear, rigid-body vehicle model.

VI. Conclusion

Initial study of the longitudinal hypersonic scramjet vehicle model under development at AFRL has revealed a rich but complex control design problem. The tight integration of propulsion and airframe presents unique challenges, and makes addressing the structural dynamics of the vehicle a critical issue. In the paper, a TLC design is presented and verified with successful trim and step response simulation on the rigid-body, longitudinal AFRL HSV model. Current work addresses the rigid body AFRL model directly, and a comparison is drawn between allocation schemes bases on lookup tables and fitted expressions. Initial simulation results are presented and show a stable controller that can fly trim flights as well as perform basic maneuvers.

VI. Acknowledgements

The Ohio University authors would like to thank the Dayton Area Graduate Studies Institute for providing funding for this project.

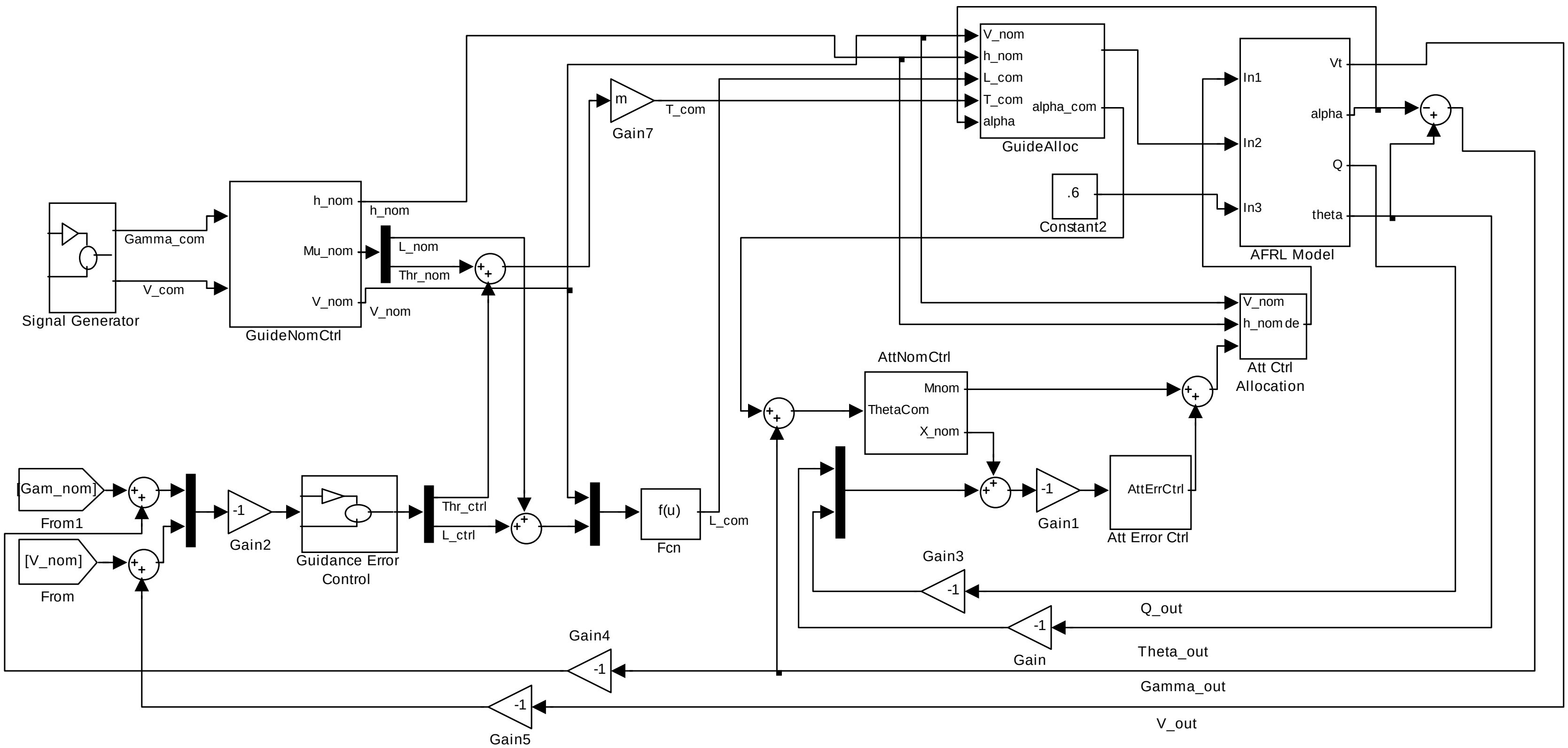

Figure 3. MATLAB/Simulink Implementation of the Rigid-Body Vehicle Model with TLC Controller

Trim Tests

In the following figures, the vehicle is trimmed at Mach 8.0 and 85,000 ft.

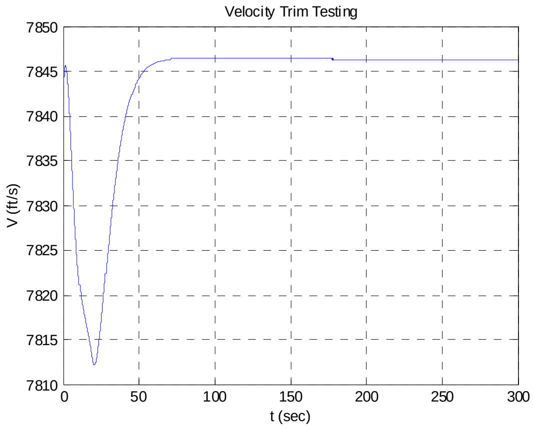

Figure 4. Velocity Trim Test

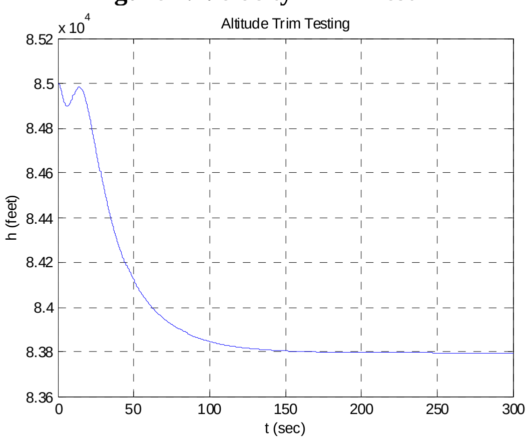

Figure 5. Altitude Trim Test

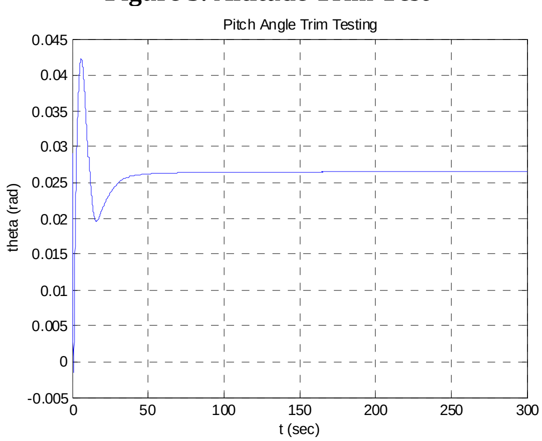

Figure 6. Pitch Angle Trim Test

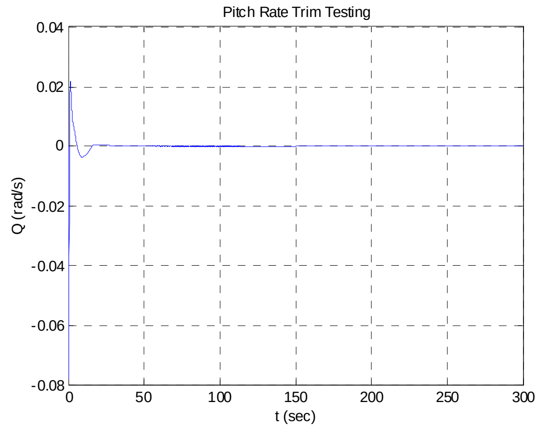

Figure 7. Pitch Rate Trim Test

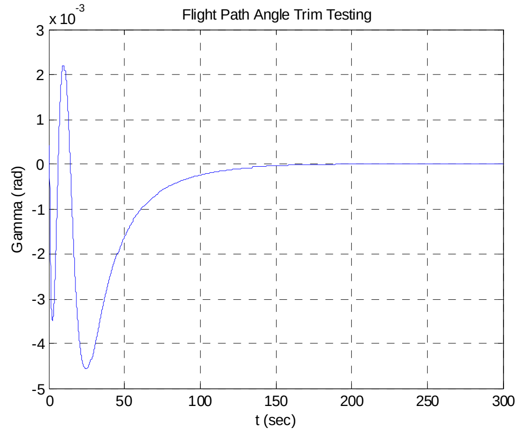

Figure 8. Flight Path Angle Trim Test

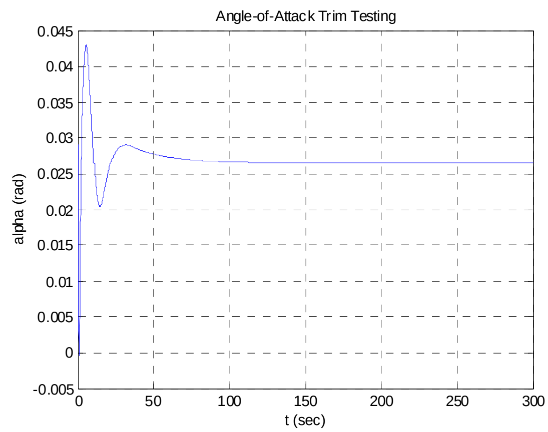

Figure 9.Angle-of-Attack Trim Test

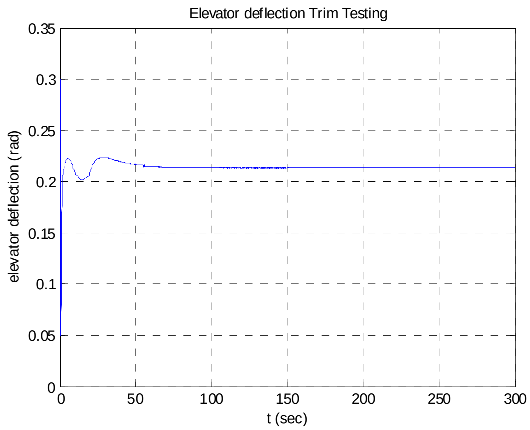

Figure 10. Elevator Deflection Trim Test

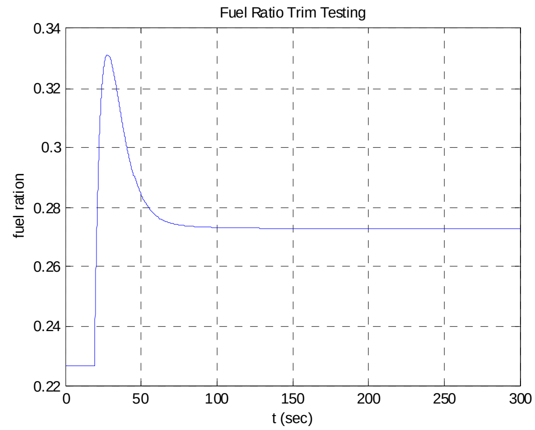

Figure 11. Fuel Ratio Trim Test

Step Response Tests

In the following figures, the vehicle is trimmed at Mach 8.0 and 85,000 ft for the first 100s, and then a step command is issued to increase the velocity by 500 ft/s.

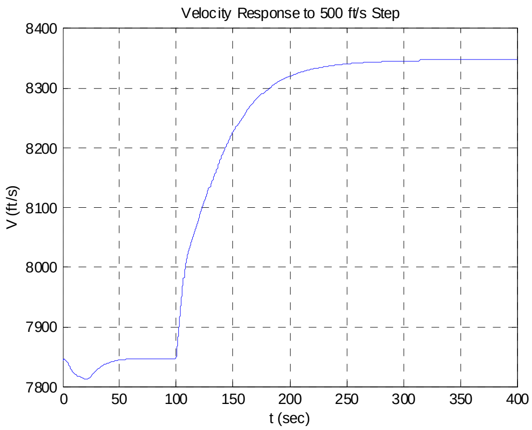

Figure 12. Velocity Response to Velocity Step Command

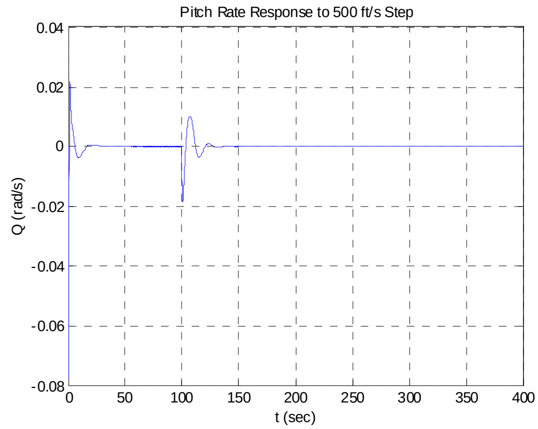

Figure 14. Pitch Rate Response to Velocity Step Command

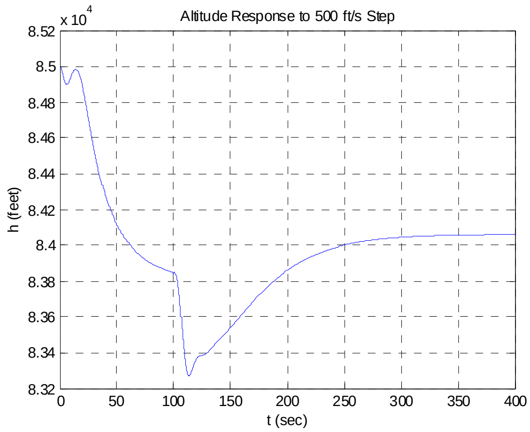

Figure 13. Altitude Response to Velocity Step Command

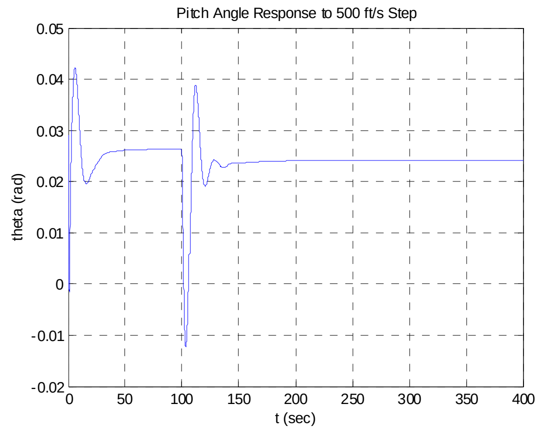

Figure 15. Pitch Angle Response to Velocity Step Command

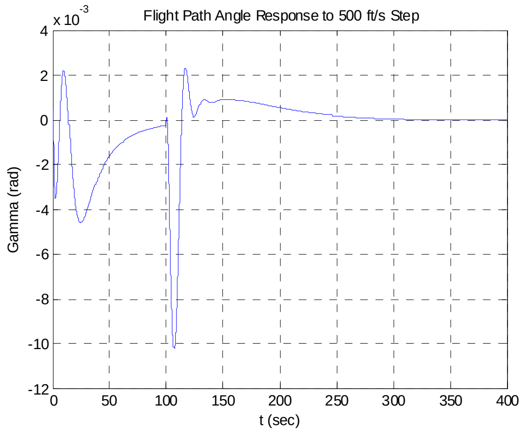

Figure 16. Flight Path Angle Response to Velocity Step Command

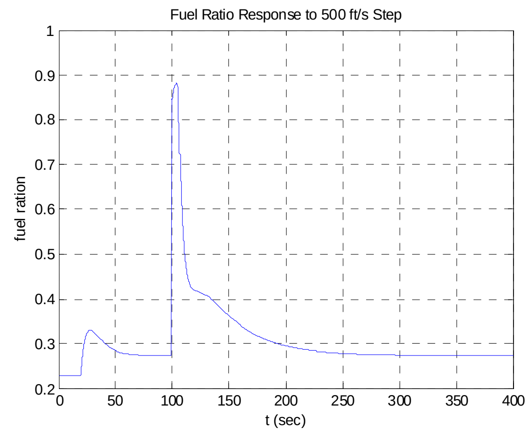

Figure 19. Fuel Ratio Response to Velocity Step Command

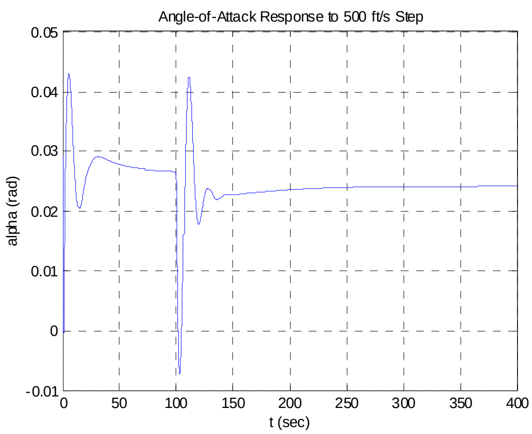

Figure 17. Angle-of-Attack Response to Velocity Step Command

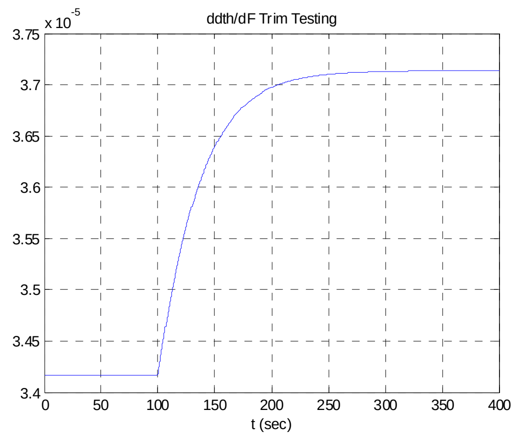

Figure 20. $\frac{d\delta_{th}}{dF}$ Response to Velocity Step Command

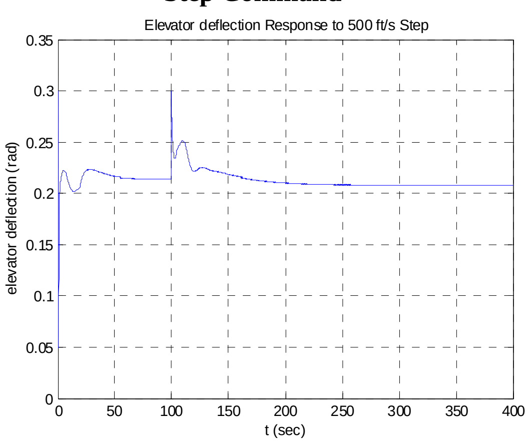

Figure 18. Elevator Deflection Response to Velocity Step Command

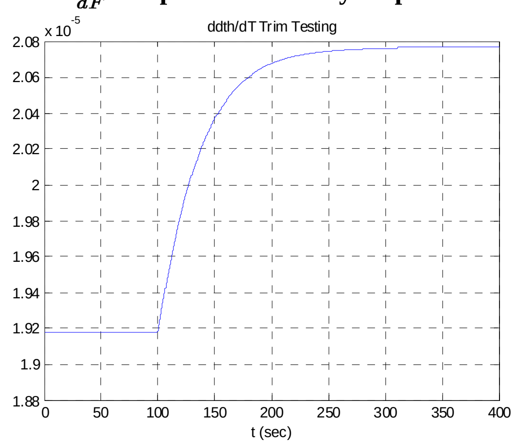

Figure 21. $\frac{d\delta_{th}}{dT}$ Step Response

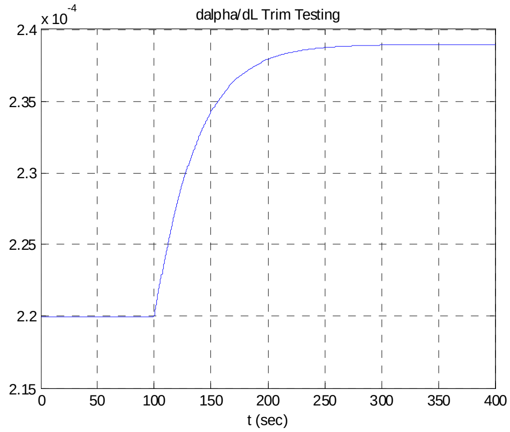

Figure 22. $\frac{d\alpha}{dL}$ **Step Response**

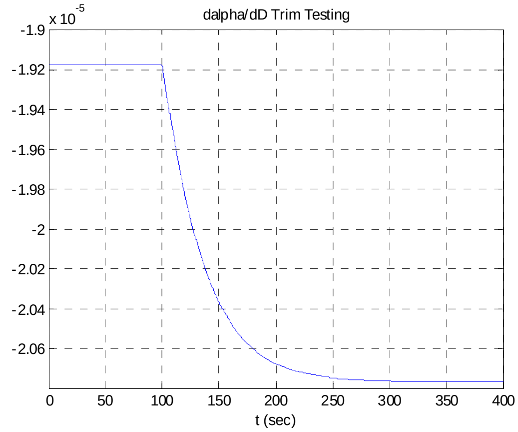

Figure 23. $\frac{d\alpha}{dD}$ **Step Response**

VIII. References.

[1]Chavez, F. R. and Schmidt, D. K., "Analytical Aeropropulsive/Aeroelastic Hypersonic-Vehicle Model with Dynamic Analysis," *AIAA Journal of Guidance, Control, and Dynamics*, Vol. 17, No. 6, 1994, pp. 1308–1319.

[2]Chavez, F. R. and Schmidt, D. K., "Uncertainty Modeling for Multivariable-Control Robustness Analysis of Elastic High-Speed Vehicles," *AIAA Journal of Guidance, Control, and Dynamics*, Vol. 22, No. 1, 1999, pp. 87–95.

[3]Bilimoria, K. D., and Schmidt, D. K., "Integrated Development of the Equations of Motion for Elastic Hyperonicd Flight Vehicles," *AIAA Journal of Guidance, Control, and Dynamics,* Vol. 18, No. 1, 1995, pp. 73-81.

[4]Bolender, M. A., and Doman, D. B. "A Non-Linear Model for the Longitudinal Dynamics of a Hypersonic Air-breathing Vehicle," *AIAA Guidance, Navigation, and Control Conference and Exhibit,* Aug. 15-18, 2005.

[5]Marrison, C. I., and Stengel, R. F., "Design of Robust Control Systems for Hypersonic Aircraft," *AIAA Journal of Guidance, Control, and Dynamics,*Vol. 21, No. 1, 1998, pp. 58-63.

[6]Wang Q., and Stengel, R. F., "Robust Nonlinear Control of a Hypersonic Aircraft," *AIAA Journal of Guidance, Control, and Dynamics,*Vol. 23, No. 4, 2000, pp. 577-585.

[7]Aouf, N, Boulet, B, and Botez, R., "A Gain Scheduling Approach for Flexible Aircraft," *Proceedings of the American Control Conference,* May 8-10, 2002, pp. 4439-4442.

[8]Calise, A. J., Kim, J., and Buffington, J. M., "Adaptive Compensation for Flexible Dynamics," *AIAA Guidance, Navigation, and Control Conference and Exhibit,* Aug 5-8, 2002.

[9]Schmidt, D. K, and Velapoldi, J. R., "Flight Dynamics and Feedback Guidance Issues for Hypersonic Airbreathing Vehicles," *AIAA Guidance, Navigation, and Control Conference and Exhibit,* Aug. 9-11, 1999.

[10] M. A. Bolender, D. B. Doman, Improving Flight Path Control In Hypersonic Vehicles, Submitted for Publication.

[11]Oppenheimer, M. W., Control of an Unstable, Non-Minimum Phase Hypersonic Vehicle Model, Submitted for Publication.

[12]J. T. Parker, P. Jankovsky, and A. Serrani, Dynamic Inversion Controller for the Bolender Model without Heave Coupling, A Presentation Given at Wright Patterson Air Force Base, August, 2005.

[13] J. Zhu, Nonlinear Tracking and Decoupling by Trajectory Linearization, Lecture Note, Presented at NASA MSFC, 137 pp., June 1998.

[14]Zhu, J., Banker, B. D., and Hall, C. E., X-33 Ascent Flight Controller Design by Trajectory Linearization, a Singular Perturbational Approach,". AIAA, Washington, D.C., 2000.

[15]Zhu, J., Hodel, A. S., Funston, K., and Hall, C. E., "X-33 Entry Flight Controller Design by Trajectory Linearization- a Singular Perturbational Approach, *Proceedings of American Astro. Soc. G&C Conf.,* 2001, pp. 151-170.

[16]Lim, T. W., and Alhassani, A. A., "On-line, Simultaneous Identification of Multiple Modes for Flexible Structures Using Adaptive Filtering Techniques. *Proceedings AIAA Guidance, Navigation, and Control Conference,* AIAA, Washington, D.C. , 1997.

[17]Taylor, R., Pratt, R. W., and Caldwell, B. D., "Improved Design Procedures in Aeroservoelasticity," *Proceedings AIAA Atmospheric Flight Mechanics Conference and Exhibit,* AIAA, Washington, D. C., 1998.

[18]Huang, R., Mickle, M. C., and Zhu, J., "Nonlinear Time-varying Observer Design Using Trajectory Linearization".